JOURNAL OF Applied Polymer SCIENCE

Influence of Processing on Morphology in Short Aramid Fiber Reinforced Elastomer Compounds

Christian Hintze,[1,2,3] Regine Boldt,[2] Sven Wiessner,[1,2] Gert Heinrich[1,2]
[1]Institut für Werkstoffwissenschaft, TU Dresden, D-01062 Dresden, Germany
[2]Leibniz-Institut für Polymerforschung Dresden e.V., D-01069 Dresden, Germany
[3]Dutch Polymer Institute DPI, P.O. Box 902, 5600 AX Eindhoven, The Netherlands
Correspondence to: C. Hintze (E-mail: hintze@ipfdd.de)

ABSTRACT: The rubber industry is nowadays facing the general increase of raw materials as the customers are confronted with rising prices for energy. Therefore there is a need for higher durability of elastomer applications. Short fiber reinforced elastomers can contribute to the improvement of dynamic and wear properties. To determine structure–property relationships in short fiber reinforced elastomer compounds it is of crucial interest to know the contributions of fiber aspect ratio, volume content, orientation and fiber–elastomer interaction. Therefore the influence of different processing conditions and fiber contents on the resulting morphology and macroscopic properties was investigated in this article by the help of fluorescence and confocal laser microscopy using a transparent ethylene-propylene-diene rubber (EPDM) matrix. It was found that the processing induced fiber breakage was the key factor in determining the composite morphology and subsequent physical properties. © 2013 Wiley Periodicals, Inc. J. Appl. Polym. Sci. 000: 000–000, 2013

KEYWORDS: elastomers; fibers; composites; properties and characterization; morphology

Received 22 January 2013; accepted 1 April 2013; Published online 00 Month 2013
DOI: 10.1002/app.39353

INTRODUCTION

Generally short fibers mixed into elastomers can contribute to the improvement of hardness,[1,2] heat build-up,[3] and wear properties[4,5] and, therefore, increase the durability of the corresponding applications. Especially the improvement of crack deflection and the achievable anisotropic properties are advantages of these high aspect ratio fillers over particulate fillers like carbon black or silica.[6] Short fiber reinforcement in elastomers can provide a substantial contribution to build more efficient and durable tires, transmission- and conveyor belts, seals and hoses.[7] To get optimal performance of those composites the following factors have to be paid attention to: sufficient dispersion of fibers, preserving a high aspect ratio during processing, controlling the orientation in the desired direction for application and sufficient interaction between fiber and the matrix. In former works natural fibers were applied, which have a low CO_2 footprint but also variable properties.[8–11] Also man-made fibers were under investigation and could show improved reinforcement, except brittle fibers like carbon and glass that undergo high breakage.[12–14] However, that short aramid fibers can offer a good reinforcement level in elastomers and thermoplastic elastomers was shown by several authors. [2–7,14–17] Because of the inertness of the aramid surface, the fibers were treated in different studies to achieve a better bond between the elastomer and the fibers.[18–22]

To verify the influence parameters the characterization of the composite morphology plays an important role, which is often hampered by the presence of carbon black in typical industrially relevant elastomer recipes. New high resolution X-ray computer tomographic techniques allow distinguishing even micrometer sized objects in carbon black filled elastomers.[23] However, because of the low density contrast between the aramid fibers and the elastomers the effort is rather high to specify the fiber morphology in a statistical way.

For these reasons in this article transparent ethylene-propylene-diene rubber (EPDM) matrix compounds were chosen to determine the separate contributions of short aramid fiber content, aspect ratio, orientation, and fiber–elastomer interaction to the ultimate composite properties.

EXPERIMENTAL

Materials

As matrix an EPDM type Keltan® 8340A (55 wt % ethylene, 39.5 wt % propylene, 5.5 wt % ethylidene norbornene) from DSM Elastomers B.V., The Netherlands was chosen. Table 1 shows the different components of the peroxide system and the fiber content in phr and vol %. Trimethylolpropane-trimethacrylate (TRIM) and Perkadox® 14/40 peroxide were obtained from AkzoNobel, Deventer, The Netherlands. Twaron®

Table 1. Compound formulation in phr

Components	EPDM	EPDM+ 1 phr PPTA	EPDM+ 3 phr PPTA	EPDM+ 5 phr PPTA
EPDM Keltan 8340A	100	100	100	100
Perkadox 14/40	1.5	1.5	1.5	1.5
TRIM	0.6	0.6	0.6	0.6
PPTA		1 *(0,6)*[a]	3 *(1,7)*	5 *(2,9)*

[a] Values in italic brackets are the corresponding fiber vol.%.

poly(para-phenylene terephtalamide) (PPTA) short fibers with a weighted initial length of 3.8 mm and a filament diameter of 12 µm were supplied by Teijin Aramid B.V., Arnhem, The Netherlands. The fibers are treated with a standard finish, which is an oily substance on the fiber surface to ease processing.[19] The corresponding volume fraction of the fibers was thus ranging from 0.6 vol % (1 phr) to 2.9 vol % (5 phr).

Processing

The compounds were prepared in two steps. In the first step the fibers were incorporated on a laboratory internal mixer or two-roll mill, respectively. On internal mixer (Haake Rheomix 610p, Thermo Fisher Scientific, Karlsruhe, Germany) half of the matrix rubber was masticated for 2 min. Then the short aramid fibers were added together with the other half of the rubber. The mixing parameters were set as follows: degree of fill of 70%, initial chamber wall temperature of 90°C, rotor speed of 40 rpm, and fiber mixing time of 6 min. Alternatively the fibers were also incorporated on a two-roll mill (Polymix 110L, Servitec Maschinenservice GmbH, Wustermark, Germany) at room temperature with roller speeds set to 17 and 14 rpm and a nip gap of 0.5 mm. The matrix was masticated for 2 min and then the fibers were incorporated for 6 min.

In the second step the incorporation of the curatives as well as the orientation of the fibers was carried out again on the two-roll mill. The general orientation of the fibers was assumed to be in the milling direction as it was reported by Senapati et al.[24] The oriented samples were then piled into the compression mold by preserving the fiber orientation and cured at 170°C for t_{90} + 2 min under pressure of 10 MPa in a heating press (Fortijne Grotnes BV, Vlaardingen, The Netherlands). As obvious from Figure 1 the overflow channels of the mold influence the orientation of the fibers. They are leading to disorientation from the milling direction (*y*-direction), especially when the samples were chosen close to the channels. The positions and the distance *x* to the overflow channels of the specimen punched out of the 2-mm-thick vulcanized rubber sheets for characterization are shown in Figure 1.

Characterization

Curing Characteristics. Curing values, like minimum and maximum torque, optimal curing time t_{90} and scorch time t_{s1} were determined with the help of rubber process analyzer (Scarabaeus SIS V50) from Scarabaeus Mess- und Produktionstechnik GmbH, Langgöns, Germany. The specimens were tested according to DIN 53523 at a temperature of 170°C with an amplitude and frequency of 0.2 and 0.83 Hz, respectively.

Mechanical Properties. The mechanical properties were determined according to DIN 53504 using a tensile testing machine (Zwick GmbH Ulm, Germany) with a cross-head speed of 200 mm min^{-1} and five S2 type tensile bars punched out in fiber direction. Tests were executed in longitudinal direction of fiber orientation, corresponding to the milling direction *y*. From the tensile test Young's modulus defined as secant modulus between 1% and 2% strain, as well as the stress and elongation were obtained.

Dynamic Mechanical Thermal Analysis. The viscoelastic mechanical properties of the vulcanizates including storage E', loss modulus E'', and loss factor tan δ were characterized in a temperature range from −80°C to 80°C in tensile mode at a heating rate of 2 K min^{-1} at a constant frequency of 10 Hz. For the measurements a dynamic mechanical analyzer, EPLEXOR 2000N (Gabo Qualimeter Testanlagen GmbH, Ahlden, Germany) was applied using a rectangular rubber vulcanizate block having an area of 35 × 10 mm^2.The influence of the deformation amplitude on the viscoelastic properties was characterized at room temperature at a frequency of 10 Hz in the range of 0.1–100%.

Morphology Analysis. The initial aspect ratio of the fibers was obtained by measuring 100 random bundles with a digital caliper. To determine the aspect ratio after processing, from every compound 15-µm-thick films were compression molded by a hot press. After that fluorescence microscopy was carried out on these films with a microscope in reflection mode (Axio Imager

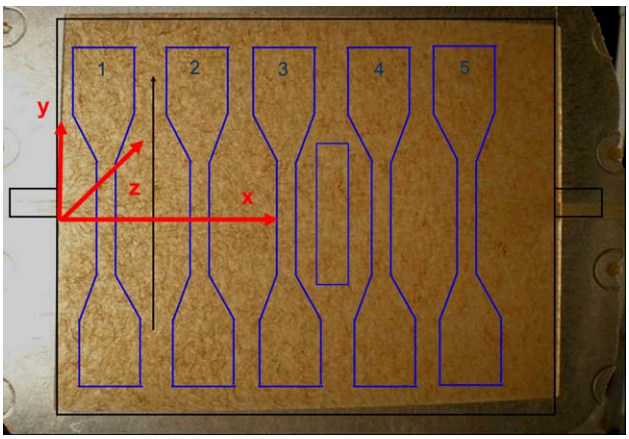

Figure 1. Vulcanized rubber sheet with numbered sampling positions. [Color figure can be viewed in the online issue, which is available at wileyonlinelibrary.com.]

A1m von Carl Zeiss Jena GmbH, Germany). Individual images of these films with a magnification of 5×, later compiled with software, were recorded. The weighted aspect ratio of about 200 fibers was then determined manually by operator according to

$$a = \frac{\sum N_i \times l_i^2}{\sum N_i \times l_i} \times \frac{1}{d} \quad (1)$$

where N_i is the number of fibers having a length l_i and d is the diameter of the fibers. Thereby fibers with a diameter less than the normal thickness of 12 μm and those touching the edge were left out. The fiber surface and failure behavior was investigated by scanning electron microscopy (SEM Ultra 55 plus, Carl Zeiss SMT, Germany) of the fracture surfaces of the tensile bars after testing. Samples were sputtered with 2 nm layer of platinum before examination.

To determine the fiber orientation in the S2 tensile bars confocal laser scanning microscopy (CLSM) was applied before the tensile test. The parallel part in the middle section of these tensile bars was then scanned with a CLSM (TCS SP5, Leica Microsystems, Wetzlar, Germany). A projection of the 3D fiber microstructure in plane 100 μm below the surface was processed by binarization. To get the autocorrelation this image was then processed by the FD Math algorithm from ImageJ software using a macro developed by Pegel et al. to detect the orientation of carbon nano tubes in polycarbonate.[25] Details can be found in the corresponding work. To obtain the main orientation angle α of the fibers in the composite with respect to direction of tensile testing and the orientation factor a binarized image was investigated with a covariance or two point probability function. The orientation factor o_f was then calculated indicating the ratio of the correlation functions at a distance r:

$$o_f = 1 - \frac{x(r)}{y(r)} \quad (2)$$

Thus the highest degree of orientation would result when o_f is equal to 1, whereas for random orientations this value would be zero.

RESULTS AND DISCUSSION

Morphology Analysis

As previously shown[26,27] aramid fibers exposed to buckling tend to fibrillate and become shortened to a significant degree, because of their superimposed microscopic and macroscopic structures, e. g. crystalline structures, pleat structures, fibrillar structures, and skin-core structures.[28] Also treatments to enhance the fiber–rubber adhesion can influence the remaining aspect ratio in the composite.[11,20] To determine the degree of fiber breakage it is important to specify the initial fiber aspect ratio. The initial weighted aspect ratio of all fibers was 315.

Figure 2 shows the investigated micrographs of the composite morphology in dependence of processing step and fiber volume content with the corresponding fiber length distributions in the graph below. The aspect ratios calculated from the weighted fiber lengths are displayed in Table 2. After processing the aspect ratio was reduced to values between 158 [1 phr Figure 2(a)] or 165 [5 phr Figure 2(c)] for fibers incorporated only by two-roll mill and 85 1 phr Figure 2(b)] or 80 [5 phr Figure 2(d)] for those incorporated by internal mixer. These results can be attributed to a higher predamage of the fibers in internal mixer, which is then amplified by the two-roll milling for orientation and adding curatives. Rajeev et al. reported similar behavior when mixing melamine fibers in EPDM.[29] Obviously also the fiber–fiber interactions were increased for a higher fiber content of 5 phr leading to mechanical interlocking of the fibers.

When short fibers are used to reinforce elastomer composites, the stress has to be transferred from the elastomer to the fiber. Assuming a perfect bond between the fiber and the elastomer at low elongations, the difference in strains along the fiber creates a shear stress distribution across the fiber–elastomer interface.[30] It is possible to calculate the minimum aspect ratio that is needed to reach the full potential of fiber strength according to a model proposed by Rosen:[31]

$$a = \left[\frac{1}{2} \times \frac{E_F}{G_M} \times \frac{1-\varphi^{1/2}}{\varphi^{1/2}}\right]^{1/2} \quad (3)$$

where E_F is elastic modulus of the fiber, G_M is the shear modulus of the matrix, whereas φ is the fiber volume content fraction.

Table 2 shows the aspect ratios calculated according to eq. (3). The measured aspect ratios were clearly below the level of the calculated ones.

Below the mean fiber diameter of 12 μm fibrils could be found. These fibrils showed lengths up to 500 μm and originated from the surface of fractured filaments. These kind of fibrils were reported by several authors and are caused by the buckling susceptibility of the fibers.[27,28]

Figure 3 shows SEM images with the two breakage mechanism that caused the fiber breakage and fibrillation. The filaments exhibited characteristic kink bands, which were induced by multiple buckling during the mixing process. This kink bands caused cracks at the skin, which were initiated by any discontinuity and led to fibrillation in filament axis [Figure 3(a)] and finally to separated fibrils. Figure 3(b) shows that when the cracks reached the whole filament diameter, fiber breakage perpendicular to filament axis occurred as reported by Konopasek et al.[27]

Figure 4 shows the surface of fractured tensile specimen with 5 phr fibers. Fiber pull-out was evident by the holes left in the elastomer matrix. The fibers sticking out the elastomer revealed no bound rubber on the fiber surfaces, which indicated that the fiber–elastomer interaction was, as expected, rather low. As shown in Table 2 the critical aspect ratios necessary for effective reinforcement were not reached by the measured ones. However, as the strength of the matrix was magnitudes under that of the fiber, the failure of the composite was initiating either in the matrix or in the fiber–elastomer bond which is in accordance with other works.[16,32]

Curing Characteristics

Table 3 shows the characteristic curing values like torque and curing times for the compounds. Generally the maximum torque values were rising with growing fiber content, whereas the initial minimum torque value was relatively unaffected. Similar

Applied Polymer SCIENCE

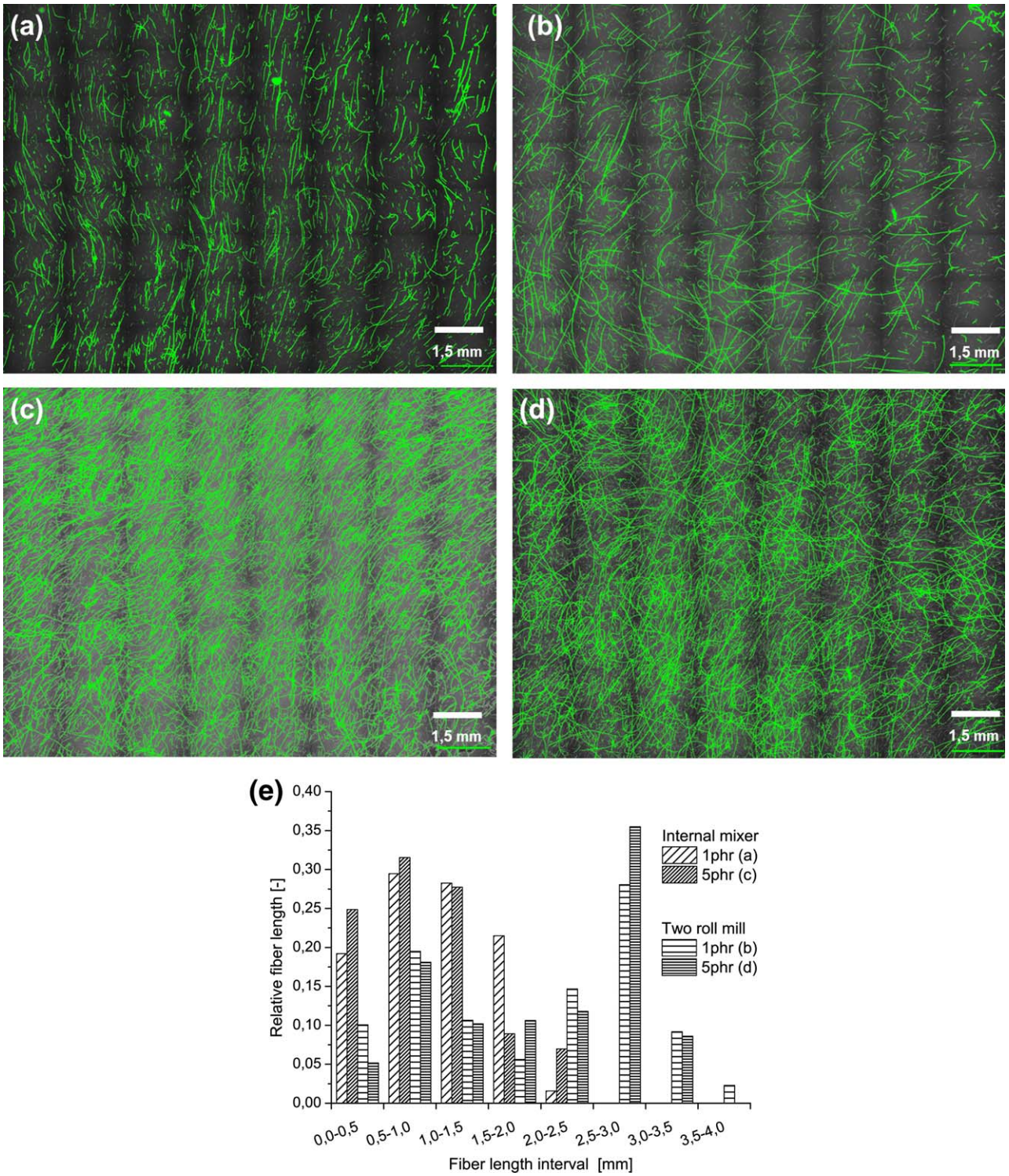

Figure 2. Thin film images for Twaron incorporated in EPDM with internal mixer (a) 1 phr and (c) 5 phr or two roll (b) 1 phr and (d) 5 phr and their corresponding fiber length distribution. [Color figure can be viewed in the online issue, which is available at wileyonlinelibrary.com.]

behavior was found for various short fiber types in elastomer matrices.[14,29,33] Especially the samples with fibers incorporated on two-roll mill showed increased maximum torque values, which can be attributed to the observed higher remaining fiber length in the compound. The optimum curing time t_{90} kept the same level for all compounds, except the specimen with 1 phr mixed on two-roll mill that showed a higher value. The scorch time t_{s1} was slightly declining with increasing fiber content. This effect could be caused by the higher thermal conductivity of the compounds induced by the faster heat transfer through the fiber–elastomer interfaces into the matrix and the higher inner friction in the compounds.

Table 2. Measured and calculated aspect ratios

	1phr		5 phr	
Incorporated by	mixer	mill	mixer	mill
Measured aspect ratio	85	158	80	165
Critical aspect ratio[a]	658	658	419	419

[a] acc. to equation 3 and based on E_f=67GPa,G_m=0,94MPa, φ= 0.0058 (1 phr) to 0.0286 (5 phr).

Mechanical Properties

The fiber orientation in the punched out S2 tensile bars is strongly dependent on the distance x of the overflow channel and therefore on the position in the mold as marked in Figure 1. Even when the fibers were originally well oriented, the overflow channels could influence the deviation angle of the milling and testing direction and the orientation factor. Figure 5(a) shows the binarized CLSM images for the middle section of the tensile specimen taken out of positions 1, 3, and 5. Fast fourier transformation was then applied to those images and the orientation predictors were examined. Figure 5(b,c) dependence of the orientation predictors α and o_f, the measured Young's modulus, and stress–strain curves from the position in the mold for a compound of 5 phr mixed via internal mixer. While getting closer to position 3, the o_f values increased, whereas α values declined. Therefore the measured Young's modulus had a maximum at position 3 and decreased when coming nearer to overflow channels. The corresponding tensile curves follow the same trend.

Figure 6 shows the influence of fiber content and mixing device on the median stress–strain behavior in fiber direction. Generally the addition of fibers induced a steeper initial slope of the stress–strain curve, whereas reducing elongation at break. As reported the aspect ratio after processing was doubled for the fibers processed only by two-roll mill compared to that incorporated on internal mixer and further processed on two-roll mill. The effect of higher fiber–matrix interface caused by the higher aspect ratio was enhancing with the increasing fiber content. So the maximum stress values and Young's modulus values were rising. Therefore Young's modulus for 5 phr processed on two-roll mill was three times higher than the value for 5 phr processed on internal mixer, whereas strain at break was reduced to values below 25%. However, above a certain elongation threshold all composites failed at the weak fiber–elastomer bond because of high stiffness differences between the matrix and the fiber.

It is possible to predict the modulus of short fiber reinforced composites with ideal short cylindrical fibers and assuming

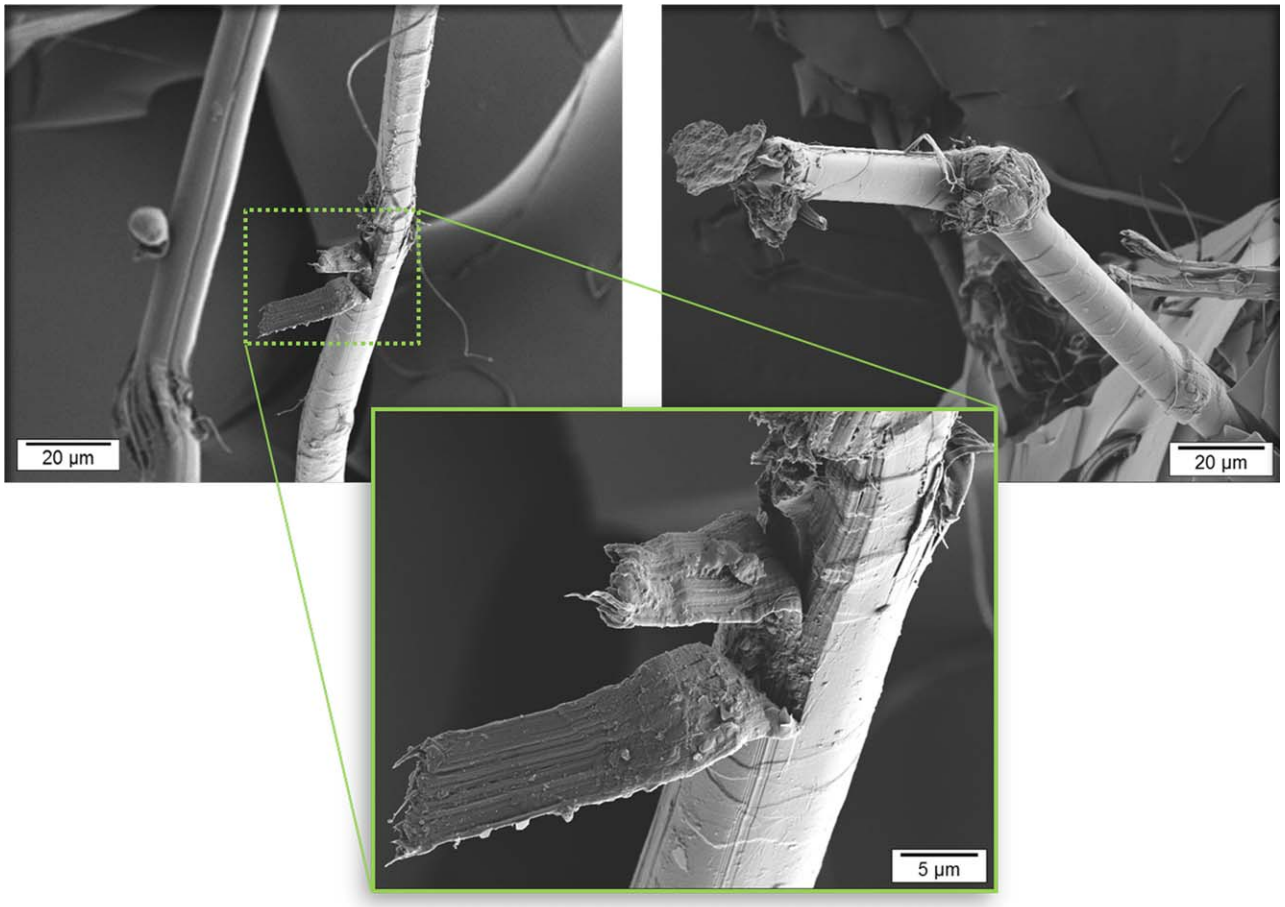

Figure 3. The two failure mechanisms: (a) skin fibrillation with zoomed detail and (b) finally fiber length reduction because of cracks through the whole diameter. [Color figure can be viewed in the online issue, which is available at wileyonlinelibrary.com.]

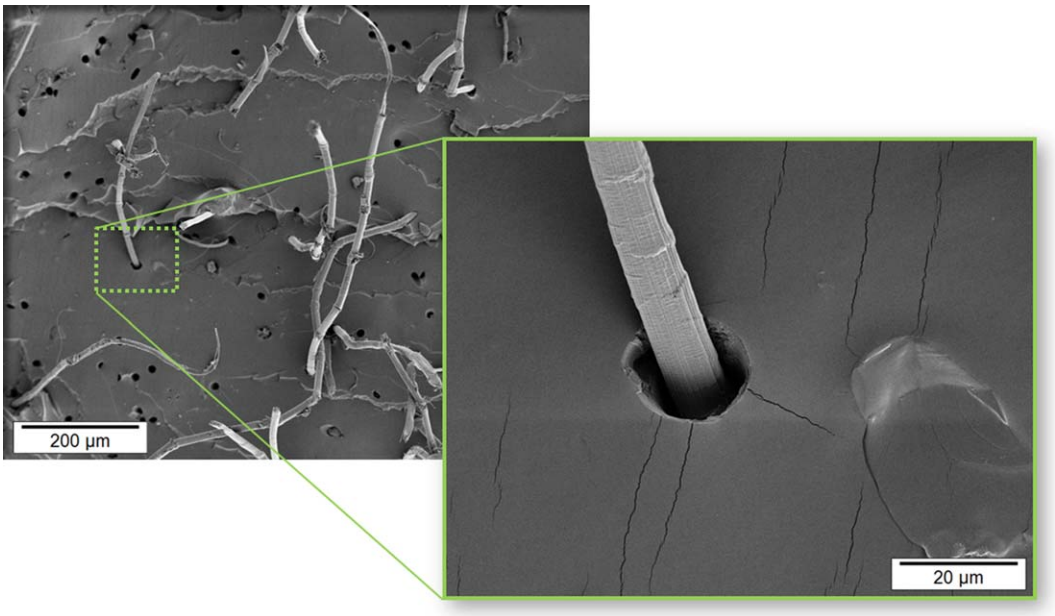

Figure 4. Surface of fractured tensile specimen with 5 phr incorporated by two roll mill with zoomed detail (fracture surface perpendicular to the milling direction *y*). [Color figure can be viewed in the online issue, which is available at wileyonlinelibrary.com.]

complete adhesion between the fibers and the matrix using the well-known Halpin–Tsai equations.[34] The following equations are needed to obtain the composites tensile modulus E_L in fiber direction:

$$E_L = E_M \times \frac{1+2a\eta\varphi}{1-\eta\varphi} \tag{4}$$

$$\eta = \frac{\frac{E_F}{E_M}-1}{\frac{E_F}{E_M}+2a} \tag{5}$$

where E_M is the tensile modulus of the matrix.

Figure 7 shows the measured Young's modulus and the calculated modulus according to the Halpin–Tsai equations in fiber direction versus fiber volume content for different ways of processing. In general the measured values stayed under the predicted trends. One reason for that might be the insufficient fiber–matrix adhesion, which is assumed to be perfect in the Halpin–Tsai model. Furthermore, the strength of the fibers was reduced by the buckling and the reduction of fiber diameter through fibrillation similar as reported by Deteresa et al.[35] As the aspect ratio was higher for the fibers incorporated on two-roll mill, also the slope of the predicted modulus was getting higher with the increasing fiber content.

Dynamic Mechanical Analysis

Figure 8(a,b) show the temperature dependent viscoelastic properties of the specimen in dependence of the mixing device and the fiber content. By adding short fibers generally the storage modulus of the composite is increased, whereas the tan δ peak at the glass transition temperature is going down.[21,36,37] Similar as for results of the tensile test, the two-roll milled specimen showed higher reinforcement in terms of storage modulus E', loss modulus E'', and reduction of tan δ peak, which can be attributed to the higher aspect ratio in the composites.

Table 3. Curing characteristics of investigated compounds

Fiber content (phr)	Minimum torque (M_L,dNm)	Maximum Torque (M_H,dNm)	M_H - M_L	Curing time (t_{90},min)	Scorch time (t_{s1}, min)
Gum	0.4	4.3	3.9	12.8	1.9
Incoporated by mixer					
1	0.4	4.6	4.1	12.8	1.8
3	0.4	4.7	4.3	13.1	1.9
5	0.5	5.1	4.6	12.9	1.8
Incorporated by two roll mill					
1	0.4	4.6	4.2	14.4	2.0
3	0.4	5.1	4.7	13.1	1.7
5	0.5	5.6	5.2	13.2	1.6

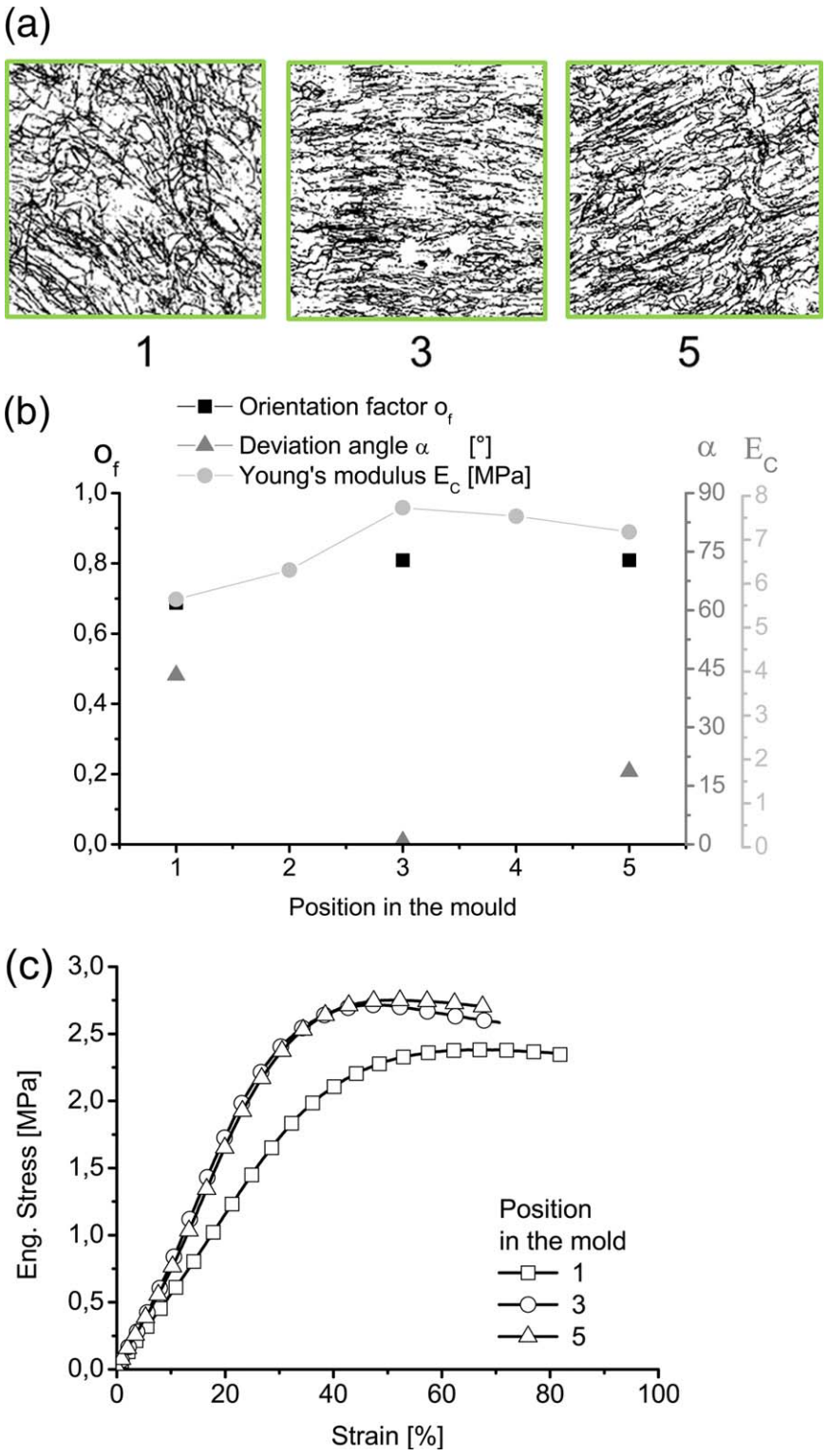

Figure 5. (a) CLSM images the tensile specimen taken out of positions 1, 3, and 5 (from the left to the right); (b) dependency of orientation predictors α and o_f, the measured Young's modulus; and (c) stress–strain curves on the position in the mold. [Color figure can be viewed in the online issue, which is available at wileyonlinelibrary.com.]

In Figure 9 the influence of deformation amplitude on the storage modulus is displayed for the different processing ways and fiber contents. As already reported the storage modulus increased for higher amounts of fiber–elastomer interface. For small amplitudes this could be confirmed. However, for dynamic strains above 1% the storage modulus of the

Applied Polymer SCIENCE

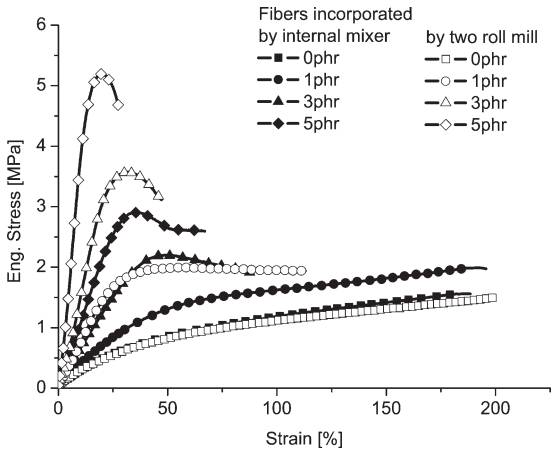

Figure 6. Stress–strain curves in fiber direction with different fiber contents and processing conditions.

composites began to fall to the level of the gum compound. This was caused by the gradual pull out of the fibers. A similar behavior was reported for EPDM filled with short polyester fibers.[38]

CONCLUSIONS

The process determined morphology of short aramid fiber filled elastomer composites was investigated in this article. Therefore, the main influence factors, like fiber aspect ratio, volume content, orientation, and fiber–elastomer interaction, were studied and correlated to the final composite properties. The aspect ratio of the aramid fibers was significantly reduced during processing. Composites processed only on a two-roll mill showed doubled remaining aspect ratios compared to that incorporated in an internal mixer. The two main mechanisms for aspect ratio change are fibrillation and fiber length reduction induced by the frequent buckling of the anisotropic fibers during mixing. The measured aspect ratios are, in general, significantly lower than the calculated minimum aspect ratios needed to utilize the full fiber strength. However, because of the high differences in stiffness and strain at break between fiber and elastomer matrix

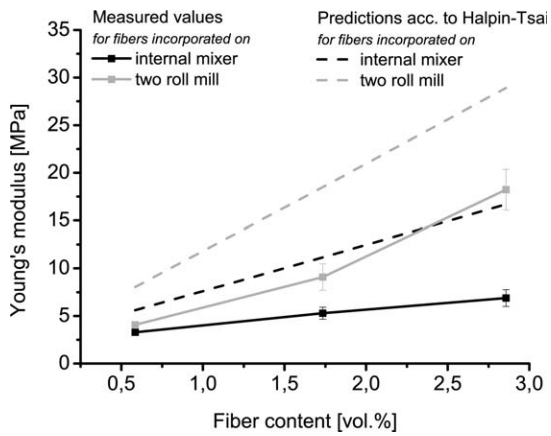

Figure 7. Measured Young's modulus and predicted modulus from Halpin-Tsai equations in fiber direction versus fiber volume content for different processing ways.

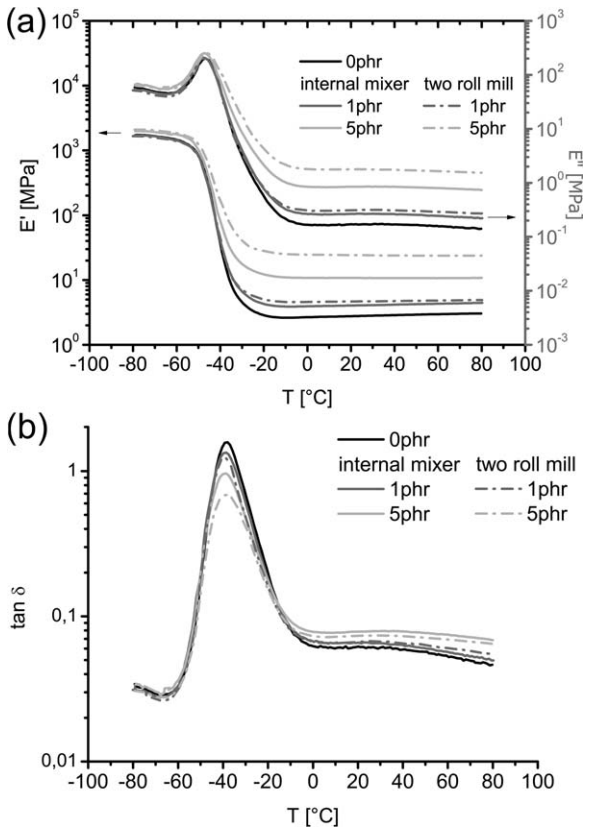

Figure 8. (a) E', E'' and (b) tan δ curves in fiber direction with respect to different fiber contents and processing conditions.

the composites fail in the fiber–elastomer interface over a certain strain level. For low strains the fiber–elastomer interface, determined by the fiber aspect ratio and volume content, influences the mechanical properties significantly. The larger the fiber–elastomer interface the higher the Young's modulus and the lower the elongation at break. The same effect is also observed for another important influence factor, the fiber orientation. The better the orientation is the steeper is the initial slope of the stress–strain curve and the lower is the strain at break. The values of Young's modulus and the orientation

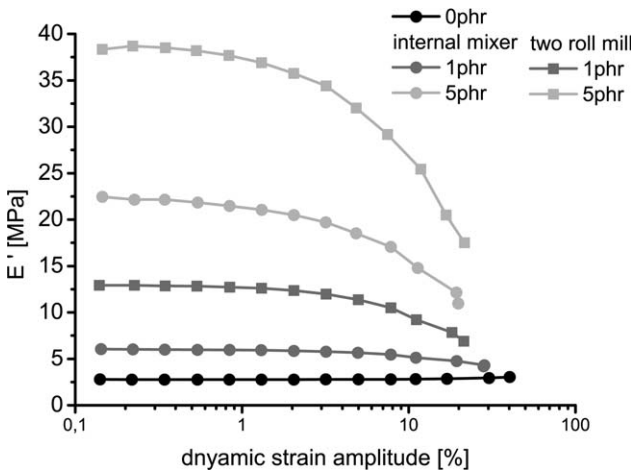

Figure 9. E' versus dynamic strain in fiber direction with respect to different fiber contents and processing conditions.

parameters derived by the CLSM investigations could confirm that the preferential milling orientation was affected by the presence of overflow channels in the mold. Similar to findings for the tensile behavior, results of dynamical mechanical analysis show that by increasing the fiber–elastomer interface, the storage modulus is increasing, whereas tan δ peak at glass transition temperature is declining. For higher dynamic strains the storage modulus of the fiber reinforced specimen decreased because of fiber pull-out.

ACKNOWLEDGEMENT

This study is part of the research program of the Dutch Polymer Institute (DPI), under project # 664. Authors gratefully acknowledge Teijin Aramid B.V. Arnhem, and DSM Elastomers B.V. Geleen, The Netherlands, for their support. The authors thank C. Drosdzol and R. Schumann (both Leibniz-Institut für Polymerforschung e.V. Dresden) for measuring the fiber aspect ratios.

REFERENCES

1. Kumar, R. P.; Thomas, S. *Bull. Mater. Sci.*, **1995**, *18*, 1021.
2. Vajrasthira, C.; Amornsakchai, T.; Bualek-Limcharoen, S. *J. Appl. Polym. Sci.*, **2003**, *87*, 1059.
3. Rijpkema, B. *Kautsch. Gummi Kunstst.*, **1994**, *47*, 748.
4. Uchiyama, Y.; Wada, N.; Iwai, T.; Ueda, S.; Sado, S. *J. Appl. Polym. Sci.*, **2005**, *95*, 82.
5. Kashani, M. R. *J. Appl. Polym. Sci.*, **2009**, *113*, 1355.
6. Kumar, R. P.; Thomas, S. *Polym. Int.*, **1995**, *38*, 173.
7. Van der Pol, J.F. *Rubber World*, **1994**, *32*, 210,
8. Setua, D. K.; De, S. K.; *J. Mater. Sci.*, **1984**, *19*, 983.
9. Chakraborty, S. K.; Setua, D. K.; De, S. K. *Rubber Chem. Technol.*, **1982**, *55*, 1286.
10. Geethamma, V. G.; Mathew, K. T.; Lakshminarayanan, R.; Thomas, S. *Polymer*, **1998**, *39*, 1483.
11. Jacob, M.; Thomas, S.; Varughese, K. T. *Compos. Sci. Technol.*, **2004**, *64*, 955.
12. Murthy, V. M.; Bhowmick, A. K.; De, S. K. *J. Mater. Sci.*, **1982**, *17*, 709.
13. Cataldo, F. *J. Macromol. Sci. Phys.*, **2008**, *47*, 818.
14. Manchado, M. A.; Arroyo, M. *Polym. Comp.*, **2002**, *23*, 666.
15. Akbarian, M.; Hassanzadeh, S.; Moghri, M. *Polym. Adv. Technol.*, **2008**, *19*, 1894.
16. O'Connor, J. E. *Rubber Chem. Technol.*, **1977**, *50*, 945.
17. Ahmad, I.; Wong, P. Y.; Abdullah, I. *Polym. Comp.*, **2006**, *27*, 395.
18. Ahmad, I.; Chin, T. S.; Cheong, C. K.; Jalar, A.; Abdullah, I. *Am. J. Appl. Sci.*, **2005**, 14.
19. de Lange, P. J.; Akker, P. G.; Willemsen, S.; Datta, R. N. *J. Adh. Sci. Technol.*, **2009**, *23*, 139.
20. Hintze, C.; Shirazi, M.; Wiessner, S.; Talma, A. G.; Heinrich, G.; Noordermeer, J. W. M. *Rubber Chem. Technol.*, accepted
21. Shirazi, M.; Talma, A. G.; Noordermeer, J. W. M. *J. Appl. Polym. Sci.*, **2012**, 1097.
22. Shibulal G. S.; Naskar K.; *Express Polym. Lett.*, **2012**, *6*, 329.
23. Alshuth, T.; Robin, S.; *Kautsch. Gummi Kunstst.*, **2010**, *9*, 383.
24. Senapaty, A. K.; Kutty, S. K. N.; Pradhan, B.; Nando, G. B. *Int. J. Polymeric. Mater.*, **1989**, *12*, 203.
25. Pegel, S.; Pötschke, P.; Villmow, T.; Stoyan, D.; Heinrich, G. *Polymer*, **2009**, *50*, 2123.
26. Hintze, C.; Heinrich, G.; Wiessner, S.; Wagenknecht, U. *Gummi Fasern Kunstst.*, **2012**, *9*, 562.
27. Konopasek, L.; Hearle, J. W. S. *J. Appl. Polym. Sci.*, **1977**, *21*, 2791.
28. Panar, M.; Avakian, P.; Blume, R. C.; Gardner, K. H.; Gierke, T. D.; Yang, H. H. *J. Polym. Sci. B Polym. Phys.*, **1983**, *21*, 1955.
29. Rajeev, R. S.; Bhowmick, A. K.; De, S. K.; Kao, G. J. P.; Bandyopadhyay, S. *Polym. Compos.*, **2002**, *23*, 574.
30. Kelly, A. R.; Tyson, W. R. *J. Mech. Phys. Solids*, **1965**, *13*, 329.
31. Rosen, B. W.; Dow, N. F. *Fracture*, **1972**, *7*, 612.
32. Clarke, J.; Harris, J. *Plast. Rubber Compos.*, **2001**, *30*, 406.
33. Lopattananon, N.; Panawarangkul, K.; Sahakaro, K.; Ellis, B. *J. Appl. Polym. Sci.*, **2006**, *102*, 1974.
34. Halpin, J. C.;Tsai, S.C. *AFML TR*, **1969**, 67.
35. Deteresa, S. J.; Allen, S.; Farris, R.; Porter, R. *J. Mater. Sci.*, **1984**, *19*, 57.
36. Ashida, M.; Noguchi, T.; Mashimo, S. *J. Appl. Polym. Sci.*, **1985**, *30*, 1011.
37. Praveen, S; Chakraborty, B. C.; Jayendran, S.; Raut, R. D.; Chattopadhyay, S. *J. Appl. Polym. Sci.*, **2009**, *111* 264.
38. Ibarra, L. *J. Appl. Polym. Sci.*, **1994**, *54*, 1721.